ELSEVIER

Neurobiology of Aging 33 (2012) 899–913

NEUROBIOLOGY OF AGING

www.elsevier.com/locate/neuaging

Changing topological patterns in normal aging using large-scale structural networks

Wanlin Zhu[a,b], Wei Wen[a,b,*], Yong He[c], Aihua Xia[d], Kaarin J. Anstey[e], Perminder Sachdev[a,b]

[a] School of Psychiatry, University of New South Wales, Sydney, Australia
[b] Neuropsychiatric Institute, Prince of Wales Hospital, Randwick, NSW, Australia
[c] State Key Laboratory of Cognitive Neuroscience and Learning, Beijing Normal University, Beijing, China
[d] Department of Mathematics and Statistics, University of Melbourne, Melbourne, Australia
[e] Centre of Mental Health Research, Australian National University, Canberra, Australia

Received 20 October 2009; received in revised form 22 June 2010; accepted 29 June 2010

Abstract

We examine normal aging from the perspective of topological patterns of structural brain networks constructed from two healthy age cohorts 20 years apart. Based on graph theory, we constructed structural brain networks using 90 cortical and subcortical regions as a set of nodes and the interregional correlations of grey matter volumes across individual brains as edges between nodes, and further analyzed the topological properties of the age-specific networks. We found that the brain structural networks of both cohorts had small-world architecture, and the older cohort (N = 374; mean age = 66.6 years, range 64–68) had lower global efficiency but higher local clustering in the brain structural networks compared with the younger cohort (N = 428; mean age = 46.7, range 44–48). The older cohort had reduced hemispheric asymmetry and lower centrality of certain brain regions, such as the bilateral hippocampus, bilateral insula, left posterior cingulated, and right Heschl gyrus, but that of the prefrontal cortex (PFC) was not different. These structural network differences may provide the basis for changes in functional connectivity and indeed cognitive function as we grow older.

Keywords: Normal aging; Magnetic resonance imaging; Connectivity; Morphometry; Grey matter volume; Small world

1. Introduction

The two main organizing principles found in the brain, i.e., segregation and integration of information processing (Friston et al., 2002; Sporns et al., 2000), provide the theoretical framework for studying the brain as a network. One approach to studying such a complex network has been the application of graph theory (Bullmore and Sporns, 2009). This theory has been used to study human brain networks from both structural and functional data. Functional brain networks have been constructed from the data of functional magnetic resonance imaging (fMRI) (Achard et al., 2006; Ferrarini et al., 2008), electroencephalography (EEG) (Rubinov et al., 2007) and magnetoencephalography (MEG) (Stam, 2004), and these show some degree of convergence. Structural networks have used regional cortical thickness or volume (Bassett et al., 2008; He et al., 2007) or diffusion tensor imaging (DTI) based fiber-tracking information (Hagmann et al., 2007) to help understand the architecture of the brain upon which any functional network must be based. Understanding the structural network is therefore a first step in explaining functional connectivity. While the large-scale connectivity structure of the human brain represents a relatively invariant characteristic (Sporns et al., 2005), the precise combinations and topological patterns may be influenced by many factors, such as genetic differences, sex, pathologies, and/or simply normal aging. The latter is the focus of this paper.

* Corresponding author. Tel.: +61 2 93823730; fax: +61 2 93823774.
E-mail address: w.wen@unsw.edu.au (W. Wen).

0197-4580/$ – see front matter © 2012 Elsevier Inc. All rights reserved.
doi:10.1016/j.neurobiolaging.2010.06.022

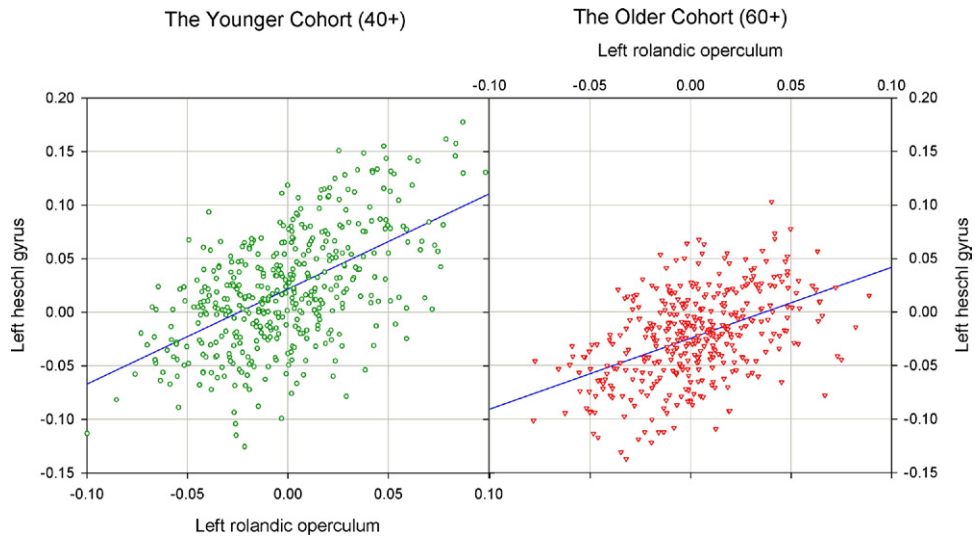

Fig. 1. The graphs show correlations between two regions (left rolandic operculum vs. left heschl gyus) in the 40+ (left) and 60+ (right) cohorts. The difference in slope is significant ($p < 0.0001$) (40+ > 60+). The 90 grey matter regions defined in this study resulted in 4,005 (90 × 89/2) possible pairs of regions for correlation. The general linear model was used with gender and scanner as fixed factors.

Most studies on human brain aging show shrinkage of the adult brain as it ages, with a reported reduction of about 5% in brain weight per decade after the age of 40 years (Kemper, 1994). However, this change is not uniform over the whole brain. Grey and white matter show different patterns of change (Raz et al., 2005). Even within the cortex, decline is most consistently reported in the superior and inferior frontal gyri and the superior temporal gyrus (Fjell et al., 2009). Other cortical regions showing age-related decline include the middle frontal gyrus, middle temporal gyri, precuneus, inferior and superior parietal cortices, fusiform and lingual gyri, and the temporo-parietal junction, but the change is less consistently seen in the inferior temporal lobe and the anterior cingulate cortex (Fjell et al., 2009; Raz et al., 2004). In general, age-associated changes are more prominent in the association cortex rather than primary cortex (Raz, 2000). Age-related changes in the white matter, which relate more to microstructural change, tend to show an anterior-posterior gradient, with frontal white matter being affected more than the temporal, parietal and occipital white matter, and the anterior part of the corpus callosum more than the posterior part (Head et al., 2004; Salat et al., 2005). These changes in the cortex and the white matter are likely to have an impact on networks between brain regions.

Aging is also related to a decline in information-processing resources, such as working memory capacity, attention regulation and processing speed, and this change is likely to be related to brain structural changes (Buckner et al., 2005). A recent study (Seeley et al., 2009) has shown strong convergence between intrinsic functional connectivity and structural covariance, with functional network maps closely mirroring cortical atrophy patterns in five neurodegenerative syndromes. Aging-related brain network changes have previously been examined from a functional (Achard and Bullmore, 2007) but not a structural perspective.

In this paper, we examine the structural brain network changes in relation to normal aging by studying two age cohorts 20 years apart. Similar to recent work (Bassett et al., 2008; He et al., 2007), we measure cortical and subcortical volumes using MRI scans, and two cortical areas are considered anatomically connected if their volumes are significantly correlated. The meaning of such coupling between cortical regions (Figure 1) is not well understood (Tootell et al., 2003), but can be further explored to look into questions, such as: when one brain region atrophies, are there correlated grey matter (GM) reductions elsewhere? Is age-related hippocampal degeneration an isolated process or is it related to degeneration elsewhere? What is the relationship of prefrontal lobe volume, another key area in aging (Resnick et al., 2003), to changes in other cortical regions? The quantitative analyses of structural brain networks allow us to look into these questions from a fresh perspective.

2. Methods

2.1. Study sample

The two cohorts of interest are part of the Personality and Total Health (PATH) through Life project (Anstey et al., 2008; Sachdev et al., 2006). PATH is a longitudinal study of three cohorts aged 20–24 (20+), 40–44 (40+) and 60–64 (60+) years, all comprising community residents recruited randomly through electoral rolls from the city of Canberra and the adjacent town of Queanbeyan, Australia. The cohorts are examined every 4 years. Enrollment to vote is compulsory for citizens of Australia, thereby making the electoral roll an excellent resource for epidemiological sam-

ples. At wave one, each cohort comprised about 2,500 individuals (the 40+ cohort = 2,354; the 60+ cohort = 2,222) who participated in an interview. The Wave two scans were used in the present study. The 20+ cohort did not have brain scans. In the 40+ and 60+ cohorts, about one in five participants were offered a brain MRI scan. In the 40+ cohort, 656 were approached and 431 underwent scans, and in the 60+ cohort the corresponding figures were 458 and 374, respectively. The reasons for not undergoing an MRI scan after having initially been selected included subsequent withdrawal of consent, medical conditions contradicting MRI, and claustrophobic or undue anxiety about the procedure. Age, gender, and years of education, along with other clinical data, were recorded during the interview. The study was approved by the ethics committees of the Australian National University, Canberra and the University of New South Wales, Sydney, Australia.

2.1.1. The younger cohort (40+)

The younger cohort comprised 431 subjects in wave 2 of the 40+ cohort who had MRI scans, but one subject's scan was lost due to an operational error, one did not have a complete protocol, and one subject was found to have a large cyst across the right occipital, posterior temporal, and parietal lobes, leading to his exclusion, thereby leaving 428 subjects (mean age = 46.7 (1.4), m/f = 197/231) for final analysis.

2.1.2. The older cohort (60+)

The older cohort comprised 374 subjects in Wave 2 of the 60+ cohort, aged 64–68 years (mean age = 66.6 (1.4), m/f = 204/170, mean MMSE = 29.35 (1.09)) at the time of examination and scanning.

2.2. MRI data acquisition

T1-weighted 3D structural scans were acquired in coronal plane on a 1.5 T Gyroscan NT Intera (ACS-NT, Philips Medical Systems, Best, Netherlands) scanner with spatial resolution of 1×1 mm^2 in-plane and 1.5 mm slice thickness. About midway through the scanning of the younger cohort, for reasons outside the researchers' control, the original scanner (scanner A) was replaced with an identical Intera Philips scanner (scanner B). Although there was a change of the scanner during the study, there was no significant alteration in acquisition parameters. The first 163 subjects of the 40+ cohort were scanned with scanner A for T1-weighted 3D structural MRI with TR = 8.84 ms, TE = 3.55 ms, flip angle = 8°, matrix size = 256 × 256 and FOV = 256, yielding in-plane resolution of 1 × 1 mm/pixel and slice thickness = 1.5 mm with no gap between slices. The acquisition parameters of T1-weighted 3D structural MRI for the remaining 268 subjects (431–163 = 268) of the 40+ cohort on scanner B were TR = 8.93 ms, TE = 3.57 ms, flip angle 8°, matrix size and FOV remained the same as scanner A, producing the same in-plane resolution and slice thickness. To ensure the reliability and compatibility of the data from the two scanners, we took three steps to examine the possible scanner impact. First, we compared the subjects of the 40+ cohort scanned on the two scanners on sociodemographic and imaging parameters. There were no differences in age ($p = 0.377$) or years of education ($p = 0.588$), but more women were inadvertently scanned on scanner B than A ($p = 0.003$). Second, we examined the volumetric measures of total intracranial volume (TIV) ($p = 0.697$), GM volume ($p = 0.934$), white matter (WM) volume ($p = 0.165$), or cerebrospinal fluid (CSF) volume ($p = 0.820$) obtained from the two scanners, and found no differences. Third, we calculated the interregional correlations of the cortical and subcortical volumes of every pair of regions for 167 subjects scanned with Scanner A and 268 subjects with Scanner B separately. The 90 grey matter regions defined (see subsections of "Computation of regional GM volume" and "Construction of structural networks") resulted in 4,005 possible pairs of regions for correlation for the subjects scanned in each scanner. No significant difference was found in any of these correlations. As the scanning of the 60+ cohort occurred after the completion of the younger cohort, they were scanned with scanner B with the identical acquisition parameters as used for the 40+ cohort scanned with scanner B.

2.3. Image preprocessing

T1-weighted structural MRI scans of both cohorts were segmented into GM, WM and CSF using SPM5 (Ashburner and Friston, 2005). The segmentation results were inspected visually. After initial rigid-body alignment of GM and WM images to achieve good intersubject scan coregistration, we applied the diffeomorphic anatomical registration through exponentiated lie algebra (DARTEL) (Ashburner, 2007), a recently published nonlinear diffeomorphic registration algorithm which notably improves the intersubject scan registration and had been implemented in SPM5 for the construction of the two cohort-specific templates (one for each age-specific cohort) of matrix size 121 × 145 × 121 and an isotropic resolution of 1.5 mm. An affine transformation from DARTEL templates to MNI-space (Evans et al., 1994) was calculated and applied to each segmented grey matter image and they were resampled with an isotropic voxel size of 2 mm. Both steps were modulated by multiplication with the determinant of Jacobian transform to preserve the GM volume.

2.4. Computation of regional GM volume

The structural networks were constructed using 90 cortical and subcortical regional GM volumes. The region names and their corresponding abbreviations are listed in Supplementary Table 1. Automated anatomical labeling (AAL) (Tzourio-Mazoyer et al., 2002) was used to define these 90 anatomical regions. We calculated the regional GM volumes for each individual GM image in the MNI space. To mask individual images, the AAL template was resa-

mpled with voxel size 2 mm and had the same direction matrix with individual images. Regional GM volume of each subject was thus calculated as the mean value of all the voxels within the region ($v_{ROI} = \frac{1}{N}\sum_{i \in ROI} v_i$) defined by AAL.

2.5. Construction of structural networks

The approach of characterizing brain connectivity using cortical connection matrices and graphs has the important advantage of an efficient and complete structural description which allows computation and comparison of different connection topologies within a common theoretical framework.

In graph theory, a network is defined as a set of nodes and the edges between them. In our work, each graph node was an anatomical region defined by the AAL template. Ninety nodes representing 90 anatomical regions (see Supplementary Table 1) were therefore employed to construct a network for each cohort. Each AAL defined regional GM volume was calculated using the general linear model to remove the effects of subjects' gender, total GM volume, and different scanners. The residuals represented regional GM volume corrected for gender, total GM volume, and scanner, which were then used for the subsequent analysis.

To obtain the edges between the nodes, we constructed the interregional correlation matrix of each cohort by calculating the partial correlation coefficients for all individuals in a cohort between the cortical/subcortical volumes of every pair of regions (nodes) (Horwitz et al., 1987; Whittaker, 1990). We use Figure 1 as an example to explain the idea of constructing one interregional correlation matrix of an entire cohort. A point (green for younger cohort or red for older cohort) shows two volumetric measures (regional grey matter volume corrected for gender, total grey matter volume, and scanner) for a participant, i.e., the volumes of left Heschl gyrus (vertical axis) and left rolandic operculum (horizontal axis) in this case. There are 428 green points (428 participants in the younger cohort) and 374 red points (374 participants in the older cohort) in Figure 1. What we were examining was the interregional correlations (between left Heschl gyrus and left rolandic operculum in this case) of the whole cohort. Therefore, only two interregional correlation matrices could be made, one for each age cohort. Each value of the matrix of the cohort represented the interregional correlation of two particular grey matter regions. This computation resulted in a pair of (90×90) partial correlations in corrected GM volumes between each of the 4,005 ($N(N-1)/2$; $N = 90$ and is the number of nodes in the graph) possible pairs of regions. We thresholded the correlation matrix with fixed sparsity which was the total number of edges in the graph divided by the maximum possible number of edges (percentage of all possible edges). A brain structural network graph could then be constructed with a binarized matrix obtained by thresholding the correlation coefficients of the interregional correlation matrix. Rather than set a static threshold, we thresholded the correlation matrix repeatedly over a wide range of sparsities and then examined the graph topological attributes of the resulting graphs at each sparsity point. This enabled us to compare the topological properties of the network graph between the two age-specific cohorts as a function of sparsity. Using the nodes and edges defined above, we constructed an unweighted and undirected graph, where each node represented a specific GM region and an edge represented the correlation between two regions.

2.6. Some networks topology properties used in the study

2.6.1. Sparsity

The degree of node i is denoted as K_i, which is the number of edges that connect it to the other nodes of the graph. Degree of a node is one of the most fundamental network measures and many network properties are based on it. Using K_i, we can then define an important parameter in our network study, the sparsity of a network. To compare the topological properties of two networks with the same number of nodes, we set the same sparsity value (for the selection of sparsity range, see 2.9 for details) for both networks so that they have the same number of edges.

2.6.2. Minimum path length and network global efficiency

The minimum (or shortest) path length L_{ij} between two nodes i and j is defined as the least number of edges that must be included to connect them. The mean minimum path length of graph L_p is defined as the average shortest path length that connects any two nodes in a network. Minimum path length is a measure of the extent of average connectivity. Therefore, global efficiency is defined as the inverse of L_p, i.e., $1/L_p$, and has been interpreted as overall routeing efficiency of the network and regarded as one of the important network properties (Latora and Marchiori, 2001).

2.6.3. Clustering coefficient and local efficiency

The clustering coefficient C_i of node i is the ratio of the number of existing edges to the number of all possible edges in the node's direct neighbors (Watts and Strogatz, 1998). The clustering coefficient for the whole network is the average clustering coefficient over all nodes in a network and is expressed as C_p. The clustering coefficient is an index of local structure, and has been interpreted as a measure of the local connectivity of a network (Bassett et al., 2008; Stam and Reijneveld, 2007). A metric E_p is also considered as a measure for local efficiency. Although both clustering coefficient and local efficiency can be used to quantify the degree of local structure of a network, they measure different aspects of local network properties. Clustering coefficient takes into account the number of triangles between a node and its neighbors, while local efficiency takes into account the ability of information transfer through the entire subgraph of a node's connections.

2.6.4. Betweenness centrality

Another metric used was the network betweenness centrality. The betweenness B_i of node i is defined as the number of shortest paths between any two nodes that run through node i (Freeman, 1977). We can then define the normalized betweenness centrality $b_i = B_i/B$ for every node, where B is the average betweenness centrality of the network. b_i is a measure that captures the influence of a node over information flow between other nodes in the network. The nodes that have high values of b_i are considered as hubs of the structural networks. The differences of the cohorts in b_i of our study reflect the aging impact on global roles of regions in the network.

In our work, L_p, C_p, and E_p of the networks were all calculated under various sparsities within the small-world regime. Therefore, a series of networks were generated at a given sparsity for the 40+ and the 60+ cohorts separately.

See Appendix for the mathematical definitions of abovementioned network properties.

2.7. Intra- and interhemispheric connections and anatomical distance

An intrahemispheric connection (or edge) is a connection between 2-g regions (nodes) in the same left or right hemisphere, and an interhemispheric connection is a connection between 2-g regions one of the right hemisphere and the other of the left hemisphere. The anatomical distance between two regions was defined as the Euclidean distance between centroids of two anatomical regions.

2.8. Small-worldness test

Small-world, characterized by a high degree of clustering and short path length linking different network nodes, is an attractive model for the description of brain networks because it not only supports both specialized and integrated information processing but also minimizes wiring costs while maximizing the efficiency of information propagation (Achard and Bullmore, 2007; Kaiser and Hilgetag, 2006; Watts and Strogatz, 1998). A network is considered a small-world network if it has almost identical path length ($\lambda = L_p^{real}/L_p^{rand} \sim 1$) but is more locally clustered ($\gamma = C_p^{real}/C_p^{rand} > 1$ and $\sigma = \gamma/\lambda > 1$) in comparison with the matched random networks (Watts and Strogatz, 1998). Therefore, to examine the small-world properties, the values of L_p^{real}, C_p^{real} of the anatomical network were compared with L_p^{rand} and C_p^{rand}, respectively. In this study, L_p^{rand} and C_p^{rand} were calculated from 2000 random networks generated using the random rewiring procedure previously described (Maslov and Sneppen, 2002; Milo et al., 2002). These randomly generated networks had the same node degree distribution as the real networks constructed using the regional GM correlations.

2.9. Small world properties of the two age-specific cohorts

Altering sparsity values of a graph would also alter the graph's structure. In this work, we used graph sparsity values rather than correlation coefficients as the thresholding values because if two graphs of the same number of nodes were constructed by using a correlation coefficient rather than a sparsity value, then the resulting graphs would contain different numbers of edges. As a result, the interpretation of topological property comparisons would be difficult and the between-group difference would not reflect the difference of the topology properties of the graphs. The lower threshold of the sparsity $K_{sparsity} \geq 1n\,(N)/(N-1)$ was used to determine the small-world regime, because the small-world properties were not estimable at a value lower than this (Achard et al., 2006; Watts and Strogatz, 1998). The upper threshold was determined as 0.31 by using the condition $\sigma > 1.1$, as more noise would be included in the network if the value was higher. Therefore, the sparsity threshold was calculated in the range of 0.051–0.31. The graph properties were systemically explored with an increment of 0.005 over this range of sparsity values.

2.10. Intra- vs. interhemispheric connections, and the prefrontal cortical anatomical distances

The networks series of both cohorts that were within the small-world regime of sparsity range (0.051–0.31) were examined. To examine the connections between the prefrontal cortex (PFC) and the other GM regions of the brain, we combined 18-g regions (i.e., dorsolateral superior frontal gyrus, middle frontal gyrus, orbital part of superior frontal gyrus, orbital part of middle frontal gyrus, opercular part of inferior frontal gyrus, triangular part of inferior frontal gyrus, orbital part of inferior frontal gyrus, medial superior frontal gyrus, and medial orbital of superior frontal gyrus of both right and left hemisphere). The average of the mean distances between each of the 18 frontal regions and the rest of brain GM regions was defined as $d = 1/18\sum_{i\in F} 1/N_i \sum_{j\in R} D_{i,j}$; where F was the union of 18 frontal regions and R the union of the rest of the regions that were connected with at least one of frontal regions and N_i was the number of connections between the frontal region i and the rest of regions under a specified sparsity.

2.11. Statistical analysis and computation implementation

All the computations were carried out by implementing algorithms using Matlab version R2008a (MathWorks, Natick, MA, USA).

2.11.1. Computation of network properties using a permutation-based approach

To test the between-cohort differences of the network properties and betweenness centrality b_i, a permutation-based approach (Bullmore et al., 1999; He et al., 2008) was

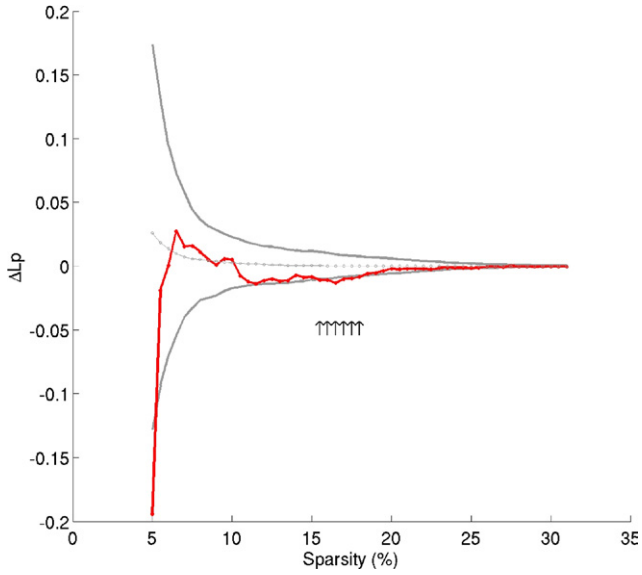

Fig. 2. Between-cohort differences in path length (L_p) as a function of sparsity. The graph shows the differences (in red, cohort 40+ minus cohort 60+) in the L_p between the 60+ and the 40+ cohorts as a function of sparsities. The grey lines represent the mean values and 95% confidence intervals of the between-group differences obtained with 2000 permutation tests at each sparsity point. The arrows indicate significant (within the sparsity range of: $0.16 \leq Ksparsity \leq 0.19$) differences in L_p between the two cohorts after correcting for multiple comparisons using FDR criterion ($p < 0.05$). Note that the older cohort has significantly larger L_p values than the younger cohort over a wide range of sparsity points.

used to find the significant differences between the cohorts. To test the null hypothesis that the observed group differences could occur by chance, we randomly reallocated each subject's set of regional GM volume measures to one or the other group and recomputed the partial correlation matrix for each randomized group. The corresponding binarized matrix was obtained using the same sparsity threshold as in the real brain networks. The network parameters were calculated for each randomized group and differences between the randomized groups were obtained. This randomization procedure was repeated 2000 times and the 95 percentile points of each distribution were used as the critical values for a one-tailed test of the null hypothesis with a probability of Type I error of 0.05 after FDR (false discovery rate) correction for the multiple comparisons (Genovese et al., 2002). The procedure was repeated at every sparsity threshold value of the brain networks. Both between-cohort difference in path length L_p as shown in Figure 2 and the between-cohort differences in clustering coefficient C_p and E_p as shown in Figure 3 were obtained in this fashion.

2.11.2. Computation of differences in regional volumes

We examined the differences in the partial correlations of mean regional GM volumes in the 40+ and 60+ cohorts. Two correlations of the same two regional GM volumes, one from each cohort, were compared, if at least one of the correlations of the pair was significant ($p < 0.05$, corrected using FDR). We used the following statistics to test the significant difference between the pair: r_1 and r_2 were the correlations of the pair; using the Fisher's r-to-z transform (Fisher, 1915), we transformed the two correlations into Z_1 and Z_2 using $Z_i = 1/21n\,(1 + r_i)/\,(1 - r_i)$, then calculated the z-statistic using $z = (Z_1 - Z_2)/\sqrt{1/(N_1-3)+1/(N_2-3)}$.

3. Results

3.1. Regional GM volume difference between the cohorts

The results in Figure 4 show that the 60+ cohort had significantly lower GM values in 86 out of 90 regions in

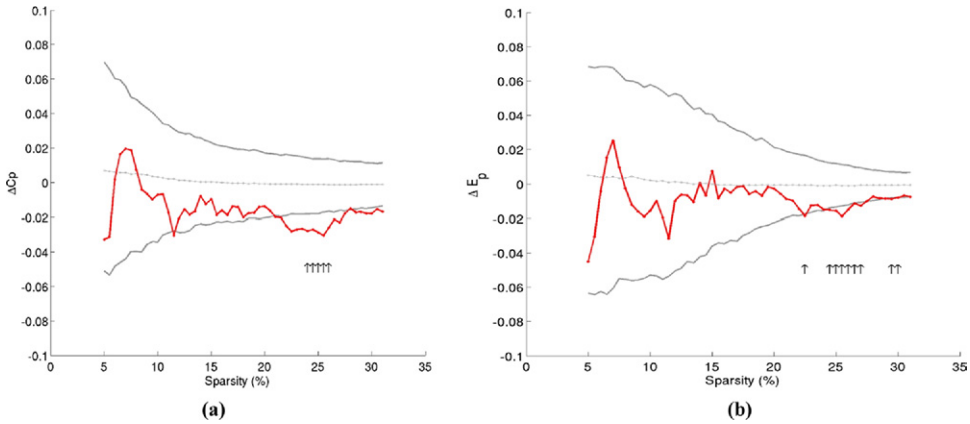

Fig. 3. Between-cohort differences in (a) clustering coefficient *Cp* and (b) local efficiency E_p as a function of sparsity. The graphs show the differences (in red, cohort 40+ minus cohort 60+) in the C_p and E_p between the older and younger cohorts as a function of sparsity thresholds. The grey lines represent the mean values and 95% confidence intervals of the between-group differences obtained with 2000 permutation tests at each sparsity value. The arrows indicate significant differences ($p < 0.05$) in C_p and E_p between the two groups after correcting for multiple comparisons using FDR criterion. Note that the older cohort show larger C_p and E_p values in the brain networks than younger cohort over a wide range of thresholds.

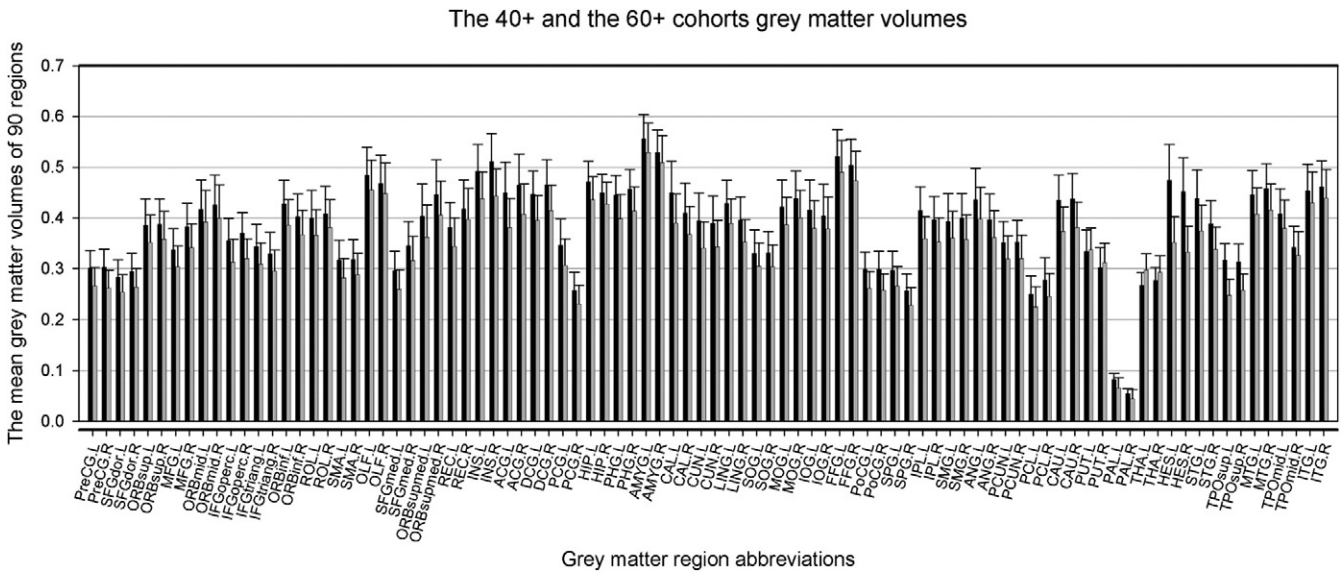

Fig. 4. Regional grey matter volume comparisons between the 40+ (black) and the 60+ (grey) cohorts. Out of 90 regions defined by AAL (Tzourio-Mazoyer et al., 2002), grey matter density was 40+ > 60+ in 86 regions, 60+ > 40+ in 3 regions (right-hand side Lenticular nucleus, putamen and thalamus of both right- and left-hand side), and 40+ = 60+ in one region (left-hand side lenticular nucleus, putamen). The multivariate general linear model was used with cohort, scanner and gender as fixed factors. More details are listed in Supplementary Table 2 and the abbreviations for the different regions are expanded in the Supplementary Table 1.

comparison with the 40+ cohort. The only three regions in which the 60+ cohort had higher GM values were right lenticular nucleus (putamen) and right and left thalamus. Left lenticular nucleus (putamen) did not show a significant difference between the two cohorts. All results were obtained with the mean regional GM volumes based on linear regression after controlling for sex and scanner effects. An FDR with $p < 0.05$ had been applied to correct for the multiple comparisons.

3.2. Correlation differences between the cohorts

As shown in Supplementary Table 3, we found three regional pairs showing significantly lower positive correlations in the 60+ cohort and one decreased negative correlation. By contrast, three anatomical region pairs were found to show increased positive correlations and seven increased negative correlations in the same older cohort in comparison with the younger cohort.

3.3. Small world properties of the two age-specific cohorts

Over the entire range of sparsity examined ($0.051 \leq K_{sparsity} \leq 0.31$), both networks had approximately equivalent shortest path length ($\lambda_p \approx 1$) and had much greater local interconnectivity ($\gamma > 1$) than the comparable random network (Watts and Strogatz, 1998) (Figure 5). Thus, both cohorts demonstrated small-world topology properties with $\sigma = (\gamma/\lambda) > 1$.

3.4. Age related structural brain network efficiency

3.4.1. Global network efficiency

Over the whole range of sparsity threshold values investigated within the small-world regime (0.051–0.31), the older cohort showed slightly but significantly longer characteristic path lengths than the younger cohort, as shown in Figure 2 using permutation test at each sparsity point (corrected for multiple comparisons with FDR criterion; $p < 0.05$, within the sparsity range: $0.16 \leq K_{sparsity} \leq 0.19$).

3.4.2. Local network efficiency and clustering coefficient

The local efficiency and clustering coefficient were examined by using two measures, i.e., E_p and C_p, respectively, as shown in Figure 5. Contrary to the reduced global efficiency in the 60+ cohort as measured with the greater minimum path lengths in comparison with the 40+ cohort, over the same range of the sparsity points within the small-world regime, both local efficiency E_p and cluster coefficients C_p of the older cohort were found to be significantly higher than the younger cohort. The cluster coefficient C_p is considered a measure of the tendency of the network elements to form local clusters. In the sparsity range $0.23 \leq K_{sparsity} \leq 0.27$, the 60+ cohort had significantly higher ($p < 0.05$; FDR corrected for multiple comparisons) C_p values. Significantly higher ($p < 0.05$; FDR corrected for multiple comparisons) E_p values were detected in some of the sparsity points within the range $0.23 \leq K_{sparsity} \leq 0.31$ in the 60+ cohort.

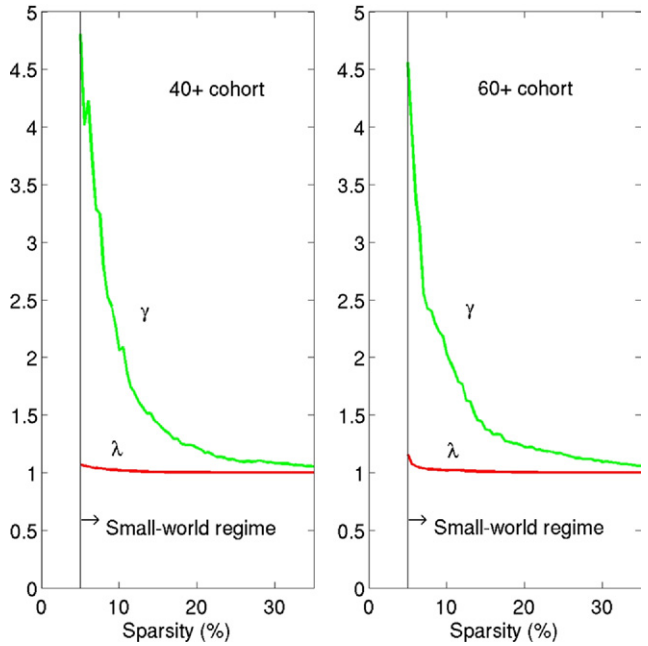

Fig. 5. Small-world properties of brain structural networks. The graphs show the changes in $\gamma = C_p^{real}/C_p^{rand}$ and $L = L_p^{real}/L_p^{rand}$ in the structural networks of both the 40+ (left panel) and the 60+ (right panel) cohorts as a function of sparsity thresholds. At a wide range of sparsity (0.051–0.31), both networks have $\gamma > 1$, $\lambda \approx 1$ (i.e., the real networks show approximately equivalent path lengths and higher clustering coefficients compared with 2000 rewiring random networks), which implies prominent small-world properties. Note that as the values of sparsity thresholds increase, the γ values decrease rapidly, but the λ values change only slightly. The arrows point to a range of sparsity in which the small-world properties are estimable because the average degrees of networks are larger than ln(*N*) (*N* is the number of nodes that represent grey matter regions).

3.4.3. GM regions with altered betweenness centrality

The GM regions with ranked betweenness centrality for both cohorts are shown in Figure 6. These GM regions were examined and the ranks were identified by using normalized nodal betweenness centrality b_i and a node (GM region) was considered a hub when its betweenness centrality was greater than 1.5. We calculated the b_i of each node of both cohorts' networks at a specific sparsity threshold of 0.061. This threshold ensured that all GM regions were included in the brain networks, i.e., there was no disconnected node in the network, while minimizing the number of false-positive paths (edges). There were 12 regions that had changed significantly in the two cohorts as shown in Supplementary Table 4. In comparison with the younger cohort, the older cohort had significant decreases in centrality in both right and left hippocampus (right hand side: the 40+ cohort: $b_i = 4.22$; the 60+ cohort: $b_i = 0.22$ $p = 0.029$; left hand side: the 40+ cohort: $b_i = 3.47$; the 60+ cohort: $b_i = 0.78$; $p = 0.01$) and insula (right hand side: the 40+ cohort: $b_i = 3.36$; the 60+ cohort: $b_i = 0.00$ $p = 0.01$; left hand side: the 40+ cohort: $b_i = 1.66$; the 60+ cohort: $b_i = 0.31$ $p = 0.049$), left posterior cingulate gyrus (the 40+ cohort: $b_i = 3.10$; the 60+ cohort: $b_i = 0.61$ $p = 0.029$) and right Heschl gyrus (the 40+ cohort: $b_i = 1.57$; the 60+ cohort: $b_i = 0.16$ $p = 0.029$). While these regions were hubs in the 40+ cohort, as their $b_i > 1.5$, they were no longer hubs in the 60+ cohort.

3.5. Intra- vs. interhemispheric connections, and the prefrontal cortical anatomical distances of the two cohorts

We found that the 60+ cohorts had more interhemispheric connections (edges) than the 40+ cohort as shown in Figure 7. Over 50% of the edges of the 60+ cohort network graphs were interhemispheric, while the 40+ cohort networks' interhemispheric connections were consistently below 50% of the total.

As shown in Figure 8, the connections between PFC and the other regions were longer for the older cohort in all sparsity values within the small-world regime.

4. Discussion

We used the correlations between regional grey matter volumes to develop a network model of the brain in two representative cohorts of healthy individuals to examine the effect of age, after correcting for possible confounding effects of sex and level of education. We found that similar to other studies (Bassett et al., 2008; Chen et al., 2008; He et al., 2007), the structural networks of both cohorts exhibited small-world characteristics. The main group differences were reduced global efficiency, increased local network clustering and reduced centrality of certain brain structures in the older cohort, in particular the bilateral hippocampus, bilateral insula, left posterior cingulate and right Heschl's gyrus.

Two cortical areas are considered anatomically connected if their volumes are significantly correlated. The meaning of such coupling between cortical regions is not well understood (Tootell et al., 2003), but this coupling could be explored in two levels. At the first level, we could directly use such concurrent brain region volume changes to examine atrophy rates and patterns (or distributions) of different populations. For example, if a region has shown age- or neurodegenerative-related atrophy and this particular region is positively correlated to a different region, then this coupling demonstrates that these two regions (for instance, the posterior cingulate/precuneus and medial temporal atrophy as found in Alzheimer's disease (AD)) are undergoing similar atrophy. Such statistical associations between brain regions were first investigated using anatomical correlations across brain regions by Lerch et al. (Lerch et al., 2006). In their study (Lerch et al., 2006), the authors proposed several measurements of assessing group differences, such as correlation slope, and correlation variance, etc. Correlation slope could be used to investigate the rate of atrophy between different brain regions among different population groups. For example, correlation slope could be used to examine whether the associated atrophy between

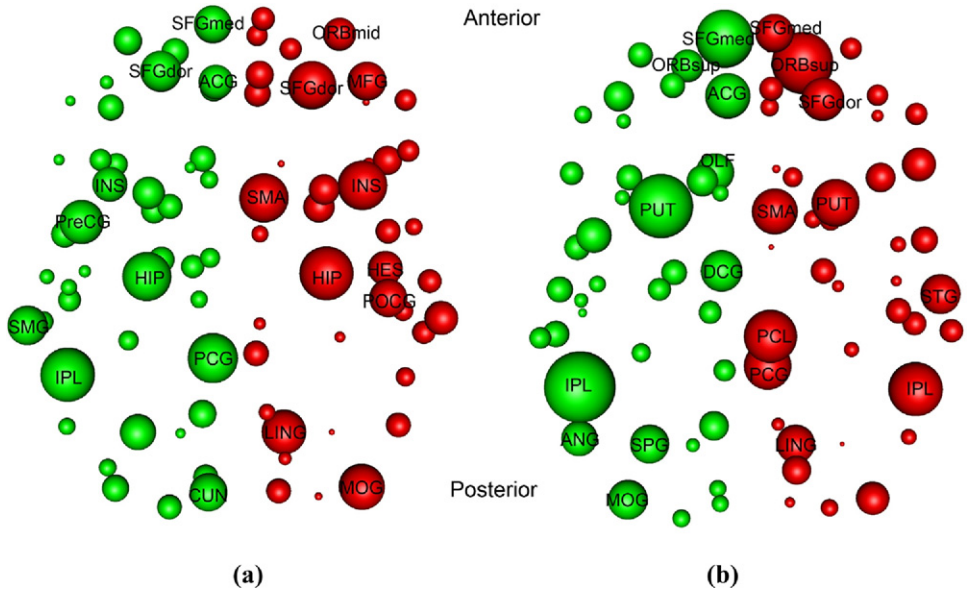

Fig. 6. Changed betweenness centrality (brains are in axial view). (a) The 40+ cohort; (b) the 60+ cohort. The radius of sphere is in proportion of the value of betweenness centrality of the region at sparsity value = 0.061, and the hubs ($b_i > 1.5$) are labeled and green nodes are left-hemispheric and red nodes are right-hemispheric. See Supplementary Table 4 for more details and the abbreviations for the different regions are expanded in the Supplementary Table 1. It is noted that the importance/connectivity of both right- and left-hand side hippocampus is reduced (from hub to non-hub) in the 60+ cohort.

posterior cingulate and medial temporal lobe changes across different age groups and/or AD and control groups. In a recent study (Seeley et al., 2009), the authors reported five different syndromic grey matter atrophy patterns in five neurodegenerative syndromes using similar methods. At the second level, we could use the quantitative analyses of structural brain networks to make sense of these concurrent brain region volume changes and relate these concurrent regional grey matter changes to functional changes for instance. This study focuses on the second level.

4.1. Reduced global network efficiency in the older cohort

The older cohort had longer characteristic path lengths for a range of sparsities, suggesting lower global network efficiency. Short path lengths have been shown to benefit effective interactions between cortical regions and subcortical areas. There is evidence that many aspects of brain anatomy can be explained in terms of minimizing axonal wiring or metabolic running cost (Achard and Bullmore, 2007; Buzsaki et al., 2004; Chklovskii et al., 2002). Interestingly, increased characteristic path lengths have also been reported in AD (He et al., 2008; Stam et al., 2004) and schizophrenia (Liu et al., 2008). In particular, normal aging and AD have some similarities in ultrastructural brain changes, including the presence of ubiquitin-immunoreactive dystrophic neurites in the cerebral cortex and granular degeneration of myelin in WM (Dickson et al., 1992). Interactions between interconnected areas of brain are believed to form the basis of cognitive processes (Friston et al., 2002). It is therefore noteworthy that an fMRI study (Achard and Bullmore, 2007) showed that while the brain functional networks were small-world and economical (Latora and Marchiori, 2001), there was a reduction of network efficiency with age.

4.2. Increased local network efficiency (clustering) in the older cohort

The older cohort demonstrated increased local efficiency, i.e., higher E_p and clustering coefficient C_p, compared with the younger cohort. Given that the small-world model reflects an optimal balance between local specialization and global integration from the graph theory point of view, the longer paths combined with higher clustering in the older cohort networks suggest a disturbance of optimal regulation, making their networks more like regular rather than random network configurations (see Figure 9). This is because a highly regular network is defined as having long path lengths and dense clustering. The increase of C_p and E_p in the aging brain network might reflect brain plasticity, in an effort to compensate for the loss of global efficiency by using direct connections between regions. More interhemispheric connections in the older cohort over the whole range of small-world regime (Figure 7) may also be a response of older age to this compensatory requirement. It has previously been reported that older adults have reduced hemispheric asymmetry (Cabeza, 2002) as demonstrated in some fMRI studies of episodic memory (Madden et al., 1999), semantic memory (Stebbins et al., 2002), working memory (Reuter-Lorenz et al., 2000), perception (Grady, 2000) and inhibitory control (Nielson et al., 2002). The higher regional

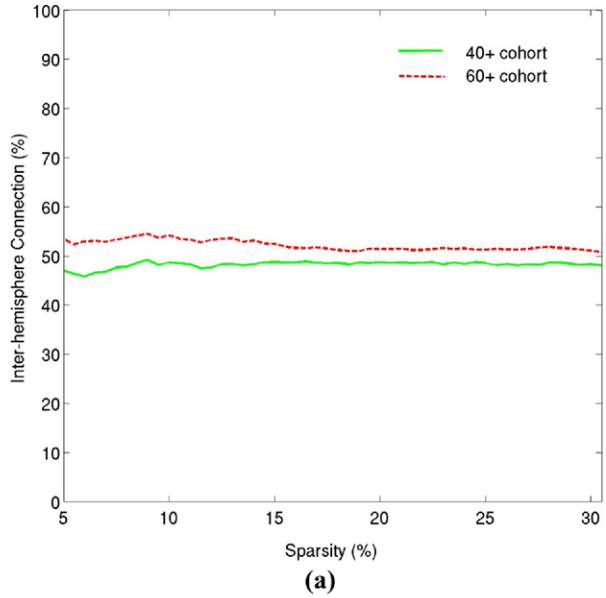

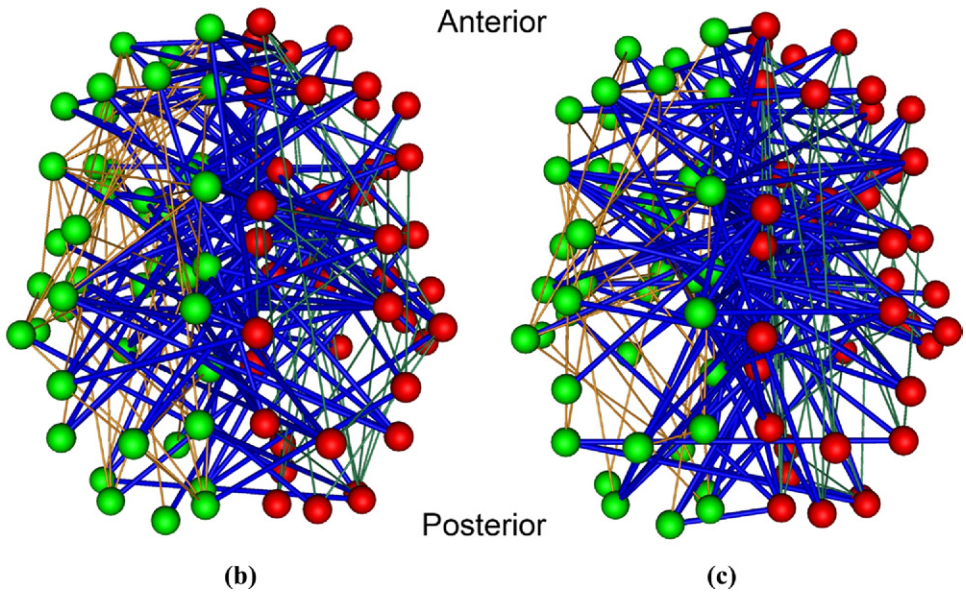

Fig. 7. (a) The percentage of inter-hemisphere connections at the sparsities within the smallworld regime. The dotted red line is the 60+ cohort and green line the 40+ cohort, and there are more inter-hemispheric connections in the older cohort than the younger cohort. The network connectivity graphs for (b) the 40+ cohort; and (c) the 60+ cohort at sparsity = 0.061 (245 edges in each graph). The blue edges are inter-hemispheric connections while the brown (left-hemispheric) and green (right-hemispheric) ones are the intra-hemispheric connections.

GM correlations and more interhemispheric connections in the older cohort would enable them to effectively recruit compensatory brain resources. It should be noted that we found significantly greater C_p and E_p values in the older cohort in the range of higher sparsity values (0.23–0.31), suggesting relatively weak correlations. This implies that with aging, declining neurobiological efficiency of the originally fine-structured networks leads to increasing reliance on a combination of compensatory processes, but these are not as efficient. The compensation in the older brain is therefore likely to entail increased cognitive effort.

4.3. Differences in betweenness centrality in the structural networks of the two cohorts

Betweenness centrality describes the importance of a particular node and its relationship with rest of the nodes in the network. Two important age-related volumetric changes are in the hippocampus and PFC. In comparison with the younger cohort, the older cohort had significantly lower centrality in both right and left hippocampi (Figure 6). Structural MRI research shows a 2–3% per decade decline in the volume of the hippocampus and parahippocampal

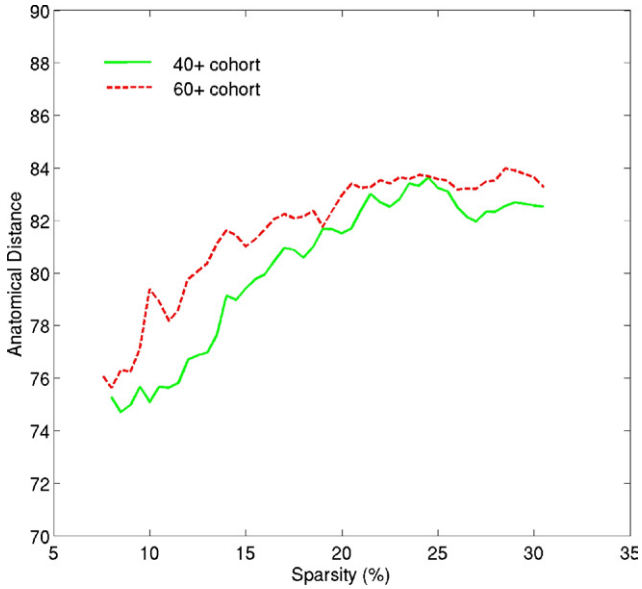

Fig. 8. The average anatomical distance between the combined frontal region (9 GM regions in each hemisphere, including dorsolateral superior frontal gyrus, middle frontal gyrus, orbital part of superior frontal gyrus, orbital part of middle frontal gyrus, opercular part of inferior frontal gyrus, triangular part of inferior frontal gyrus, orbital part of inferior frontal gyrus, medial superior frontal gyrus, and medial orbital of superior frontal gyrus) and other brain GM regions under various sparsity values within the small-world regime. Red line is the 60+ cohort and green line the 40+ cohort.

gyrus (Hedden and Gabrieli, 2004), and after the age of 60, hippocampal volume tends to predict explicit memory performance (Rosen et al., 2003). The findings in fMRI studies of reduced activity in hippocampus with aging (Daselaar et al., 2003; Mitchell et al., 2000; Park et al., 2003) are consistent with our findings.

There was no evidence of reduced betweenness centrality of the PFC for the older cohort. Given that structures of PFC undergo the largest age-related volumetric changes in adulthood, with an estimated average linear decline of about 5% per decade (Resnick et al., 2003) after the age of 20, this is an unexpected finding. PET and fMRI studies show that older adults sometimes have increased activity in PFC regions compared with younger adults (Cabeza, 2002; Grady et al., 1998). Older adults experience greater difficulty than younger adults in performing executive processes if they fail to achieve this increase (Hedden and Gabrieli, 2004). PFC is one of the more flexible structures in the brain, and compensatory processes in the aged brain may largely reside in it (Park and Reuter-Lorenz, 2009), which may explain the lack of alteration of betweenness centrality of this region with aging. The increased anatomical length of connections between PFC and the rest of brain regions in the 60+ cohort (see Figure 8), may indicate the extended compensatory efforts in the older cohort.

4.4. Biological basis of the age-related network

A number of local and global morphological changes occur in the brain with aging and these may underlie the network differences. At the local level, dendritic arbors and dendritic spines of the pyramidal neurons undergo regression with aging in specific cortical regions and layers (Duan et al., 2003). These are associated with loss of myelinated axons in the deeper layers of the cortex and the white matter (Peters et al., 2000). This is likely to affect local and global corticocortical circuits. The changes in white matter with age include reduction in volume and the appearance of signal hyperintensities suggestive of ischemic change, both seen more in the anterior brain regions (Head et al., 2004; Wen and Sachdev, 2004). How these anatomical changes translate into network efficiency is however difficult to predict, as there are likely to be both functional and structural compensations. One example of possible functional compensation is the increased activation of the PFC associated with reduced hippocampal/parahippocampal activations during memory tasks in older people (Gutchess et al., 2005). Our structural data are consistent with the functional compensation hypothesis to explain this observation. Our results also support the suggestion that older brains have a greater degree of bilaterality (Cabeza, 2002). It is also in line with the "compensatory scaffolding" hypothesis (Park and Reuter-Lorenz, 2009) which posits that additional circuits are recruited by the aging brain to shore up the declining circuits whose functioning has become noisy and inefficient. Creating scaffolds is suggested to be an active process throughout life, but in old age this may be acceler-

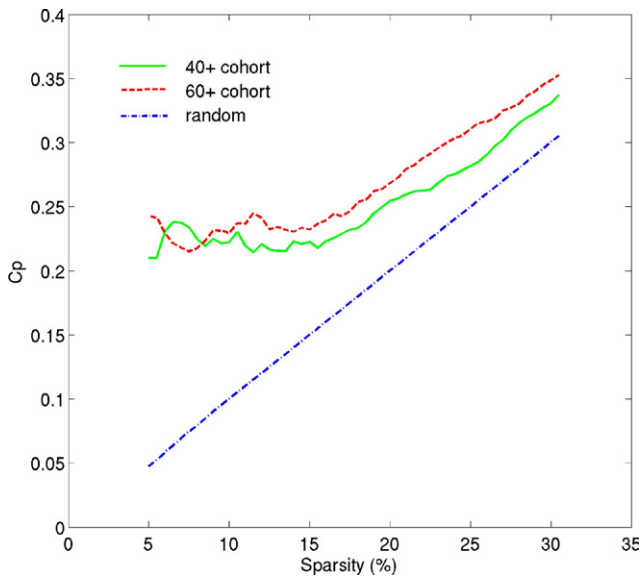

Fig. 9. (a) Clustering coefficients under various sparsities within the small-world regime (0.051–0.31). The 40+ cohort's C_p values are shown in green solid line, and the 60+ cohort in red dotted line. The figure also shows the mean clustering coefficients from 100 random graphs with blue line.

ated as a compensatory mechanism. Scaffolds are not merely functional entities, but may have an underlying structural change. However, the use of scaffolds is less efficient than the finely honed network of a younger brain.

A network approach provides the scaffolding for the computational architectures that mediate cognitive functions. It is therefore reasonable to assume that the behavioral consequences of damaging a network will reflect the disruption of the computational architecture it supports (Mesulam, 2009). In a review article, Buckner et al. (Buckner et al., 2008) observed that there was a convergence of the anatomy of the default network which comprised multiple interacting hubs. The six hubs listed (Buckner et al., 2008) were ventral medial PFC, posterior cingulate, inferior parietal lobule, lateral temporal cortex, dorsal medial PFC and hippocampal formation. In our study, we have shown (Supplementary Table 4) that three (inferior parietal lobule, hippocampus and posterior cingulate) of these six hubs had significantly decreased betweenness centrality in the older cohort in comparison with the younger cohort. Several default-mode regions, such as the posterior cingulate, inferior parietal lobule and hippocampus were found to have decreased activity in aging in resting-state activity fMRI (Andrews-Hanna et al., 2007; Damoiseaux et al., 2008).

Most of the topological changes in brain networks that have been observed so far, as reported in the literature, were associated with disease progression, experience-dependent plasticity and aging (Bullmore and Sporns, 2009). Structural changes, e.g., due to aging and neurodegenerative diseases, place constraints on which functional interactions occur in the network, i.e., the dynamics of functional networks reflect underlying structural changes. Seeley et al. (Seeley et al., 2009) hypothesized that the functionally correlated brain regions would show correlated grey matter volumes across healthy subjects. They have shown strong convergence between healthy intrinsic functional connectivity, and structural covariance measured using local region of interest (ROI) mean grey matter intensities. Furthermore, in their study of subjects diagnosed as AD, bvFTD (behavioral variant frontotemporal dementia), SD (semantic dementia), PNFA (progressive nonfluent aphasia), and CBS (corticobasal syndrome), the authors (Seeley et al., 2009) reported that functional network maps closely mirrored the atrophy patterns seen in these five neurodegenerative syndromes.

We have also noticed that brain networks share the topological properties of small-world networks, be it functional networks constructed from the data of fMRI (Achard et al., 2006; Ferrarini et al., 2008), EEG (Rubinov et al., 2008), MEG (Stam, 2004), etc. or structural networks using regional cortical thickness/volume (Bassett et al., 2008; He et al., 2007) or DTI fiber-tracking information (Hagmann et al., 2007). Structural and functional networks are related as evidenced by the fact that they share many common topological features, such as modules and hubs. However, discovering that brain networks are small-world networks is only the first step towards a comprehensive understanding of how these networks are organized and how they generate complex dynamics.

Some recent studies have shown that the modularity of structural networks can determine the hierarchical organization of functional networks (Muller-Linow et al., 2008). A resting-state fMRI study (Achard and Bullmore, 2007) reported that older people had a reduced network efficiency compared with younger population. Similar findings using structural networks were reported (He et al., 2008), i.e., when comparing AD patients with healthy controls, AD patients had lower network efficiency. A question of interest for our study is whether our findings of age-related alterations in the structural networks can be related to functional alterations as reported in the literature.

4.5. Limitations of this study

Our study has several limitations. First, unlike functional imaging data, such as fMRI, EEG, or MEG, which can yield a network for a single subject, the anatomical connectivity matrix used here is estimated on the basis of interregional correlations in a group of subjects. Second, our conclusions are based on the examination of two cohorts only, about 20 years apart in age. Even though PATH is a longitudinal study of three cohorts aged 20–24, 40–44 (40+) and 60–64 (60+) years, the youngest cohort did not have brain scans. As a result, only two cohorts with narrow age range were used in our study. Aging effects are best determined in a longitudinal study of the same cohort to avoid cohort effects. However, it has been shown that while changes in cortical thickness can be observed as early as the third decade of life, they are most obvious by the sixth decade (Salat et al., 2005). Our study therefore demonstrates the change from middle age to early old age. This is also the period that vascular risk factors are likely to become increasingly prominent, and these factors have been related to changes in cortical volume (Raz et al., 2005). Third, true structural connectivity should be supported by fiber-tracking, e.g., using DTI, to demonstrate a physical connection between two cortical regions that are correlated with each other. It is possible that correlations between cortical regions may emerge even if they are not directly connected, either by their connectivity to a third region, or because of shared mechanisms in development or degeneration. Our results therefore need support from studies using DTI for the network analysis. Additionally, the structural network should be related to the functional network obtained by fMRI data in the same individuals.

5. Conclusions

Our data suggest that structurally the brain is a network with small-world properties, and the network properties change with age, showing reduced global network efficiency, increased local network clustering and the reduced

importance of several default regions (e.g., hippocampus, posterior cingulate and inferior parietal lobule) as hubs. Aging reduces hemispheric asymmetry, which is consistent with the functional data suggesting increased bilateral activation in older individuals. The centrality of the PFC is not diminished with age, which may reflect brain plasticity. The morphological basis of changes in the network are not fully understood, but it is likely that age-associated ultrastructural changes, such as loss of dendritic length and density, changes in synaptic activity and axonal changes may contribute. These structural network changes may provide the basis for changes in functional connectivity and indeed cognitive function as we grow older.

Disclosure statement

There are no actual or potential conflicts of interest, including any financial, personal or other relationships with other people or organizations within 3 years of beginning the work submitted that could inappropriately influence our work.

Acknowledgments

This research was supported by Australian Research Council (ARC DP-0774213), National Health and Medical Research Council (NHMRC Projects 157125, 179805, 366756), the Natural Science Foundation of China (NSFC 30870667), and International Research Collaboration Scheme (IRCS) of UNSW. The study was approved by the ethics committees of the Australian National University, Canberra and the University of New South Wales, Sydney, Australia. We thank the study participants, personality and total health (PATH) Interviewers, Patricia Jacomb, Karen Maxwell, Bryan Rodgers, Helen Christensen and Tony Jorm.

Appendix 1. Mathematical expressions of network topology properties used in this study

Computation of network topology properties

We provide brief definitions for each of the graph metrics employed in this study.

A graph G defined in our work was composed of nodes, and unweighted and undirected connected edges, where each node represented a specific GM region and an edge represented the correlation between two regions.

The degree of node i is denoted as K_i, which is the number of edges that connect it to the other nodes of the graph. Using K_i, we can then define an important parameter in our network study, the sparsity of a network:

$$K_{sparsity} = \frac{1}{N(N-1)} \sum_{i \in G} K_i; \quad (A.1)$$

Where N is the number of nodes in the graph G.

The minimum (or shortest) path length $L_{i,j}$ between two nodes i and j is defined as the least number of edges that must be included to connect them. The mean minimum path length of graph is defined as the average shortest path length that connects any two nodes in a network. However the definition becomes problematic because if there is no connection between two nodes i and j, we would have $L_{i,j} \to \infty$. To address this problem, we used the "harmonic mean" distance between pairs of nodes proposed by (Newman, 2003), which is defined as:

$$L_p = \frac{N(N-1)}{\sum_{i \neq j \in G} (1/L_{i,j})}. \quad (A.2)$$

Obviously, the nodes that are not connected make no contribution to the equation.

The clustering coefficient of a node is the ratio of the number of existing edges to the number of all possible edges in the node's direct neighbors (Watts and Strogatz, 1998):

$$C_i = \frac{P_{G_i}}{K_i(K_i-1)/2}; \quad (A.3)$$

where G_i is the subgraph which consists of all the direct neighbors of the ith node, and P_G is the number of edges in the subgraph G_i. The clustering coefficient for the whole network C_P is then defined as the average clustering coefficient over all nodes in a network:

$$C_p = \frac{1}{N} \sum_{i \in G} C_i. \quad (A.4)$$

A metric also considered as a measure for local efficiency about node i is defined as (Latora and Marchiori, 2001):

$$E_i = \frac{1}{N_{G_i}(N_{G_i}-1)} \sum_{j \neq k \in G_i} \frac{1}{L_{j,k}}; \quad (A.5)$$

where N_G is the number of nodes in the subgraph G_i. The mean local efficiency of a graph is then the average of all the local efficiencies of the nodes in the graph:

$$E_p = \frac{1}{N} \sum_{i \in G} E_i. \quad (A.6)$$

An intrahemispheric connection (or edge) is a connection between 2-g regions (nodes) in the same left or right hemisphere, and an interhemispheric connection is a connection between 2-g regions one of the right hemisphere and the other of the left hemisphere. The percentage of interhemispheric connections is calculated as $2\sum_{i \in LEFT, j \in RIGHT} e_{i,j} / (\sum_{i \neq j \in G} K_i)$; where LEFT and RIGHT represent regions within the left or right hemisphere respectively, and $e_{i,j}$ is the connection between node i and node j. $e_{i,j} = 0$; if nodes i and j are not directly connected; and $e_{i,j} = 1$; if nodes i and j are directly connected. The anatomical distance between two regions was defined as the Euclidean distance between centroids of two anatomical regions i and j.

Appendix. Supplementary data

Supplementary data associated with this article can be found, in the online version, at doi:10.1016/j.humimm.2008.03.038.

References

Achard, S., Bullmore, E., 2007. Efficiency and cost of economical brain functional networks. PLoS Comput. Biol. 3, e17.

Achard, S., Salvador, R., Whitcher, B., Suckling, J., Bullmore, E., 2006. A resilient, low-frequency, small-world human brain functional network with highly connected association cortical hubs. J. Neurosci. 26, 63–72.

Andrews-Hanna, J.R., Snyder, A.Z., Vincent, J.L., Lustig, C., Head, D., Raichle, M.E., Buckner, R.L., 2007. Disruption of large-scale brain systems in advanced aging. Neuron 56, 924–935.

Anstey, K.J., Low, L.-F., Christensen, H., Sachdev, P., 2008. Level of cognitive performance as a correlate and predictor of health behaviors that protect against cognitive decline in late life: The path through life study. Intelligence 37, 600–606.

Ashburner, J., 2007. A fast diffeomorphic image registration algorithm. Neuroimage 38, 95–113.

Ashburner, J., Friston, K.J., 2005. Unified segmentation. Neuroimage 26, 839–851.

Bassett, D.S., Bullmore, E., Verchinski, B.A., Mattay, V.S., Weinberger, D.R., Meyer-Lindenberg, A., 2008. Hierarchical organization of human cortical networks in health and schizophrenia. J. Neurosci. 28, 9239–9248.

Buckner, R.L., Andrews-Hanna, J.R., Schacter, D.L., 2008. The brain's default network: anatomy, function, and relevance to disease. Ann. N.Y. Acad. Sci. 1124, 1–38.

Buckner, R.L., Snyder, A.Z., Shannon, B.J., LaRossa, G., Sachs, R., Fotenos, A.F., Sheline, Y.I., Klunk, W.E., Mathis, C.A., Morris, J.C., Mintun, M.A., 2005. Molecular, structural, and functional characterization of Alzheimer's disease: evidence for a relationship between default activity, amyloid, and memory. J. Neurosci. 25, 7709–7717.

Bullmore, E., Sporns, O., 2009. Complex brain networks: graph theoretical analysis of structural and functional systems. Nat. Rev. Neurosci. 10, 186–198.

Bullmore, E.T., Suckling, J., Overmeyer, S., Rabe-Hesketh, S., Taylor, E., Brammer, M.J., 1999. Global, voxel, and cluster tests, by theory and permutation, for a difference between two groups of structural MR images of the brain. IEEE Trans. Med. Imaging 18, 32–42.

Buzsaki, G., Geisler, C., Henze, D.A., Wang, X.J., 2004. Interneuron Diversity series: Circuit complexity and axon wiring economy of cortical interneurons. Trends Neurosci. 27, 186–193.

Cabeza, R., 2002. Hemispheric asymmetry reduction in older adults: the HAROLD model. Psychol. Aging 17, 85–100.

Chen, Z.J., He, Y., Rosa-Neto, P., Germann, J., Evans, A.C., 2008. Revealing modular architecture of human brain structural networks by using cortical thickness from MRI. Cereb. Cortex 18, 2374–2381.

Chklovskii, D.B., Schikorski, T., Stevens, C.F., 2002. Wiring optimization in cortical circuits. Neuron 34, 341–347.

Damoiseaux, J.S., Beckmann, C.F., Arigita, E.J., Barkhof, F., Scheltens, P., Stam, C.J., Smith, S.M., Rombouts, S.A., 2008. Reduced resting-state brain activity in the "default network" in normal aging. Cereb. Cortex 18, 1856–1864.

Daselaar, S.M., Veltman, D.J., Rombouts, S.A., Raaijmakers, J.G., Jonker, C., 2003. Neuroanatomical correlates of episodic encoding and retrieval in young and elderly subjects. Brain 126, 43–56.

Dickson, D.W., Crystal, H.A., Mattiace, L.A., Masur, D.M., Blau, A.D., Davies, P., Yen, S.H., Aronson, M.K., 1992. Identification of normal and pathological aging in prospectively studied nondemented elderly humans. Neurobiol. Aging 13, 179–189.

Duan, H., Wearne, S.L., Rocher, A.B., Macedo, A., Morrison, J.H., Hof, P.R., 2003. Age-related dendritic and spine changes in corticocortically projecting neurons in macaque monkeys. Cereb. Cortex 13, 950–961.

Evans, A.C., Collins, D.L., Mills, S.R., Brown, E.D., Kelly, R.L., Peters, T.M., 1994. 3D statistical neuroanatomical models from 305 MRI volumes. IEEE Nuclear Science Symposium and Medical Imaging Conference, pp. 1813–1817.

Ferrarini, L., Veer, I.M., Baerends, E., van Tol, M.J., Renken, R.J., van der Wee, N.J., Veltman, D.J., Aleman, A., Zitman, F.G., Penninx, B.W., van Buchem, M.A., Reiber, J.H., Rombouts, S.A., Milles, J., 2008. Hierarchical functional modularity in the resting-state human brain. Hum. Brain Mapp.

Fisher, R.A., 1915. Frequency distribution of the values of the correlation coefficient in samples of an indefinitely large population. Biometrika 10, 507–521.

Fjell, A.M., Westlye, L.T., Amlien, I., Espeseth, T., Reinvang, I., Raz, N., Agartz, I., Salat, D.H., Greve, D.N., Fischl, B., Dale, A.M., Walhovd, K.B., 2009. High consistency of regional cortical thinning in aging across multiple samples. Cereb. Cortex 19, 2001–2012.

Freeman, L., 1977. A set of measures of centrality based upon betweenness. Sociometry 40, 35–41.

Friston, K.J., Glaser, D.E., Henson, R.N., Kiebel, S., Phillips, C., Ashburner, J., 2002. Classical and Bayesian inference in neuroimaging: applications. Neuroimage 16, 484–512.

Genovese, C.R., Lazar, N.A., Nichols, T., 2002. Thresholding of statistical maps in functional neuroimaging using the false discovery rate. Neuroimage 15, 870–878.

Grady, C.L., 2000. Functional brain imaging and age-related changes in cognition. Biol. Psychol. 54, 259–281.

Grady, C.L., McIntosh, A.R., Bookstein, F., Horwitz, B., Rapoport, S.I., Haxby, J.V., 1998. Age-related changes in regional cerebral blood flow during working memory for faces. Neuroimage 8, 409–425.

Gutchess, A.H., Welsh, R.C., Hedden, T., Bangert, A., Minear, M., Liu, L.L., Park, D.C., 2005. Aging and the neural correlates of successful picture encoding: frontal activations compensate for decreased medial-temporal activity. J. Cogn. Neurosci. 17, 84–96.

Hagmann, P., Kurant, M., Gigandet, X., Thiran, P., Wedeen, V.J., Meuli, R., Thiran, J.P., 2007. Mapping human whole-brain structural networks with diffusion MRI. PLoS ONE 2, e597.

He, Y., Chen, Z., Evans, A., 2008. Structural insights into aberrant topological patterns of large-scale cortical networks in Alzheimer's disease. J. Neurosci. 28, 4756–4766.

He, Y., Chen, Z.J., Evans, A.C., 2007. Small-world anatomical networks in the human brain revealed by cortical thickness from MRI. Cereb. Cortex 17, 2407–2419.

Head, D., Buckner, R.L., Shimony, J.S., Williams, L.E., Akbudak, E., Conturo, T.E., McAvoy, M., Morris, J.C., Snyder, A.Z., 2004. Differential vulnerability of anterior white matter in nondemented aging with minimal acceleration in dementia of the Alzheimer type: evidence from diffusion tensor imaging. Cereb. Cortex 14, 410–423.

Hedden, T., Gabrieli, J.D., 2004. Insights into the ageing mind: a view from cognitive neuroscience. Nat. Rev. Neurosci. 5, 87–96.

Horwitz, B., Grady, C.L., Schlageter, N.L., Duara, R., Rapoport, S.I., 1987. Intercorrelations of regional cerebral glucose metabolic rates in Alzheimer's disease. Brain Res. 407, 294–306.

Kaiser, M., Hilgetag, C.C., 2006. Nonoptimal component placement, but short processing paths, due to long-distance projections in neural systems. PLoS Comput. Biol. 2, e95.

Kemper, T.L., 1994. Neuroanatomical and neuropathological changes during aging and dementia. In: Albert, M.L., Knoefel, J.E, editors. Clinical Neurology of Aging. Oxford University Press, New York, NY.

Latora, V., Marchiori, M., 2001. Efficient Behavior of Small-World Networks. Phys Rev Lett. 87, 198701.

Lerch, J.P., Worsley, K., Shaw, W.P., Greenstein, D.K., Lenroot, R.K., Giedd, J., Evans, A.C., 2006. Mapping anatomical correlations across

cerebral cortex (MACACC) using cortical thickness from MRI. Neuroimage 31, 993–1003.
Liu, Y., Liang, M., Zhou, Y., He, Y., Hao, Y., Song, M., Yu, C., Liu, H., Liu, Z., Jiang, T., 2008. Disrupted small-world networks in schizophrenia. Brain 131, 945–961.
Madden, D.J., Turkington, T.G., Provenzale, J.M., Denny, L.L., Hawk, T.C., Gottlob, L.R., Coleman, R.E., 1999. Adult age differences in the functional neuroanatomy of verbal recognition memory. Hum. Brain Mapp. 7, 115–135.
Maslov, S., Sneppen, K., 2002. Specificity and stability in topology of protein networks. Science 296, 910–913.
Mesulam, M., 2009. Defining neurocognitive networks in the BOLD new world of computed connectivity. Neuron 62, 1–3.
Milo, R., Shen-Orr, S., Itzkovitz, S., Kashtan, N., Chklovskii, D., Alon, U., 2002. Network motifs: simple building blocks of complex networks. Science 298, 824–827.
Mitchell, K.J., Johnson, M.K., Raye, C.L., D'Esposito, M., 2000. fMRI evidence of age-related hippocampal dysfunction in feature binding in working memory. Brain Res. Cogn. Brain Res. 10, 197–206.
Muller-Linow, M., Hilgetag, C.C., Hutt, M.T., 2008. Organization of excitable dynamics in hierarchical biological networks. PLoS Comput. Biol. 4 e1000190.
Newman, M.E.J., 2003. The Structure and Function of Complex Networks. SIAM. ReView 45, 167–256.
Nielson, K.A., Langenecker, S.A., Garavan, H., 2002. Differences in the functional neuroanatomy of inhibitory control across the adult life span. Psychol. Aging 17, 56–71.
Park, D.C., Reuter-Lorenz, P., 2009. The adaptive brain: aging and neurocognitive scaffolding. Annu. Rev. Psychol. 60, 173–196.
Park, D.C., Welsh, R.C., Marshuetz, C., Gutchess, A.H., Mikels, J., Polk, T.A., Noll, D.C., Taylor, S.F., 2003. Working memory for complex scenes: age differences in frontal and hippocampal activations. J. Cogn. Neurosci. 15, 1122–1134.
Peters, A., Moss, M.B., Sethares, C., 2000. Effects of aging on myelinated nerve fibers in monkey primary visual cortex. J. Comp. Neurol. 419, 364–376.
Raz, N., 2000. Aging of the brain and its impact on cognitive performance: integration of structural and functional findings In: Craik, F.I.M., Salthouse, T.A., editors. The Handbook of Aging and Cognition. Erlbaum, Hillsdale, NJ.
Raz, N., Lindenberger, U., Rodrigue, K.M., Kennedy, K.M., Head, D., Williamson, A., Dahle, C., Gerstorf, D., Acker, J.D., 2005. Regional brain changes in aging healthy adults: general trends, individual differences and modifiers. Cereb. Cortex 15, 1676–1689.
Raz, N., Rodrigue, K.M., Head, D., Kennedy, K.M., Acker, J.D., 2004. Differential aging of the medial temporal lobe: a study of a five-year change. Neurology 62, 433–438.
Resnick, S.M., Pham, D.L., Kraut, M.A., Zonderman, A.B., Davatzikos, C., 2003. Longitudinal magnetic resonance imaging studies of older adults: a shrinking brain. J. Neurosci. 23, 3295–3301.
Reuter-Lorenz, P.A., Jonides, J., Smith, E.E., Hartley, A., Miller, A., Marshuetz, C., Koeppe, R.A., 2000. Age differences in the frontal lateralization of verbal and spatial working memory revealed by PET. J. Cogn. Neurosci. 12, 174–187.
Rosen, A.C., Prull, M.W., Gabrieli, J.D., Stoub, T., O'Hara, R., Friedman, L., Yesavage, J.A., deToledo-Morrell, L., 2003. Differential associations between entorhinal and hippocampal volumes and memory performance in older adults. Behav. Neurosci. 117, 1150–1160.
Rubinov, M., Knock, S.A., Stam, C.J., Micheloyannis, S., Harris, A.W., Williams, L.M., Breakspear, M., 2007. Small-world properties of nonlinear brain activity in schizophrenia. Hum. Brain Mapp. 30, 403–16.
Rubinov, M., McIntosh, A.R., Valenzuela, M.J., Breakspear, M., 2008. Simulation of Neuronal Death and Network Recovery in a Computational Model of Distributed Cortical Activity. Am. J. Geriatr. Psychiatry. 17, 210–217.
Sachdev, P.S., Anstey, K.J., Parslow, R.A., Wen, W., Maller, J., Kumar, R., Christensen, H., Jorm, A.F., 2006. Pulmonary function, cognitive impairment and brain atrophy in a middle-aged community sample. Dement. Geriatr. Cogn. Disord. 21, 300–308.
Salat, D.H., Tuch, D.S., Greve, D.N., van der Kouwe, A.J., Hevelone, N.D., Zaleta, A.K., Rosen, B.R., Fischl, B., Corkin, S., Rosas, H.D., Dale, A.M., 2005. Age-related alterations in white matter microstructure measured by diffusion tensor imaging. Neurobiol. Aging 26, 1215–1227.
Seeley, W.W., Crawford, R.K., Zhou, J., Miller, B.L., Greicius, M.D., 2009. Neurodegenerative diseases target large-scale human brain networks. Neuron 62, 42–52.
Sporns, O., Tononi, G., Kotter, R., 2005. The human connectome: A structural description of the human brain. PLoS Comput. Biol. 1, e42.
Stam, C.J., 2004. Functional connectivity patterns of human magnetoencephalographic recordings: a "small-world" network? Neurosci. Lett. 355, 25–28.
Stebbins, G.T., Carrillo, M.C., Dorfman, J., Dirksen, C., Desmond, J.E., Turner, D.A., Bennett, D.A., Wilson, R.S., Glover, G., Gabrieli, J.D., 2002. Aging effects on memory encoding in the frontal lobes. Psychol. Aging 17, 44–55.
Tootell, R.B., Tsao, D., Vanduffel, W., 2003. Neuroimaging weighs in: Humans meet macaques in "primate" visual cortex. J. Neurosci. 23, 3981–3989.
Tzourio-Mazoyer, N., Landeau, B., Papathanassiou, D., Crivello, F., Etard, O., Delcroix, N., Mazoyer, B., Joliot, M., 2002. Automated anatomical labeling of activations in SPM using a macroscopic anatomical parcellation of the MNI MRI single-subject brain. Neuroimage 15, 273–289.
Watts, D.J., Strogatz, S.H., 1998. Collective dynamics of "small-world" networks. Nature 393, 440–442.
Wen, W., Sachdev, P., 2004. The topography of white matter hyperintensities on brain MRI in healthy 60 to 64-year-old individuals. Neuroimage 22, 144–154.
Whittaker, J., 1990. Graphical Models in Applied Multivariate Statistics. John Wiley & Sons, New York.